J Physiol Sci (2011) 61:267–278
DOI 10.1007/s12576-011-0144-0

ORIGINAL PAPER

# ATP hydrolysis-dependent asymmetry of the conformation of CFTR channel pore

**Oleg V. Krasilnikov · Ravshan Z. Sabirov · Yasunobu Okada**

Received: 9 March 2011 / Accepted: 20 March 2011 / Published online: 3 April 2011


**Abstract** Despite substantial efforts, the entire cystic fibrosis transmembrane conductance regulator (CFTR) protein proved to be difficult for structural analysis at high resolution, and little is still known about the actual dimensions of the anion-transporting pathway of CFTR channel. In the present study, we therefore gauged geometrical features of the CFTR $Cl^-$ channel pore by a nonelectrolyte exclusion technique. Polyethylene glycols with a hydrodynamic radius ($R_h$) smaller than 0.95 nm (PEG 300–1,000) added from the intracellular side greatly suppressed the inward unitary anionic conductance, whereas only molecules with $R_h \leq 0.62$ nm (PEG 200–400) applied extracellularly were able to affect the outward unitary anionic currents. Larger molecules with $R_h = 1.16$–$1.84$ nm (PEG 1,540–3,400) added from either side were completely excluded from the pore and had no significant effect on the single-channel conductance. The cut-off radius of the inner entrance of CFTR channel pore was assessed to be $1.19 \pm 0.02$ nm. The outer entrance was narrower with its cut-off radius of $0.70 \pm 0.16$ nm and was dilated to $0.93 \pm 0.23$ nm when a non-hydrolyzable ATP analog, 5′-adenylylimidodiphosphate (AMP-PNP), was added to the intracellular solution. Thus, it is concluded that the structure of CFTR channel pore is highly asymmetric with a narrower extracellular entrance and that a dilating conformational change of the extracellular entrance is associated with the channel transition to a non-hydrolytic, locked-open state.

**Keywords** CFTR · Channel pore · Conformational change · Nonelectrolyte exclusion technique · Single-channel recording

## Introduction

Cystic fibrosis transmembrane conductance regulator (CFTR), also called ABCC7, shares structural similarities with many others of the ATP-binding cassette (ABC) family of proteins: it has two cytoplasmic, nucleotide-binding domains (NBDs) to bind and hydrolyze ATP, two transmembrane domains (TMDs) consisting of six membrane-spanning α-helices each and the cytoplasmic regulatory domain (RD) that connects CFTR's two homologous halves, TMD1/NBD1 and TMD2/NBD2 [1–7]. As with other ABCC subfamily members, only the second of the nucleotide-binding domains (NBD2) is hydrolytic in CFTR [8].

Unlike other ABC transporters that are ATP-hydrolyzing pumps for active transport of nutrients, drugs and solutes across the membrane [7], CFTR is an ATP-gated $Cl^-$ channel, in which the two processes, binding of ATP and channel gating, are allosterically coupled. CFTR is

O.V. Krasilnikov and R.Z. Sabirov contributed equally to this work.

O. V. Krasilnikov · R. Z. Sabirov · Y. Okada (✉)
Department of Cell Physiology, National Institute for Physiological Sciences, Okazaki 444-8585, Japan
e-mail: okada@nips.ac.jp

O. V. Krasilnikov
Department of Biophysics and Radiobiology, Federal University of Pernambuco, Recife, PE 50670-901, Brazil

R. Z. Sabirov
Laboratory of Molecular Physiology, Institute of Physiology and Biophysics, Academy of Science RUz, Niyazova 1, 100095 Tashkent, Uzbekistan

R. Z. Sabirov
Department of Biophysics, National University, Niyazova 1, 100095 Tashkent, Uzbekistan

dependent on PKA-mediated phosphorylation of RD, and its ATPase activity facilitates the conformational change of the protein from open to closed states [3–5, 8, 9]. The cytoplasmic two NBDs of CFTR channel may, at least transiently, form a head-to-tail heterodimeric complex with two ATP molecules sandwiched at the dimer interface [6, 10–12]. It is acceptable that ATP dissociation or hydrolysis at any of the sites triggers dimer dissociation. Such dynamic NBD dimerization serves as the molecular mechanism that couples ATP binding and hydrolysis cycles to cyclic changes in the TMDs. The conformational signals generated by NBD heterodimer formation and dissociation are transmitted to the TMDs where they result in opening and closing, respectively, of the CFTR ion-permeation pathway. Hydrolysis of ATP does not appear to be essential to either channel opening or closing transition per se but enables repeated cycles of gating to occur because the release the products (ADP and $P_i$) allows the cycle to be accomplished rapidly [8, 13, 14].

Flow of anions through the CFTR channel is indispensable to the normal function of the fluid-secreting epithelia of airways, intestine, pancreas, testes and sweat glands, and mutations in the CFTR gene are a cause of cystic fibrosis [2, 4, 15–18]. The mechanisms of anion permeation through the CFTR pore have been functionally well studied [19–21], and the recent structural and biochemical studies have provided mechanistic insight to the CFTR channel function [4, 12, 22]. However, the structure–function relationship of the CFTR pore is still poorly understood. The entire CFTR protein proved to be difficult for structural analysis at high resolution. The situation is further complicated because the CFTR channel might exhibit multiple conductance and/or functional states [23–25]. So, despite substantial efforts, including the development of homologous and atomic models of the three-dimensional structure of CFTR in both open and closed states [4, 22, 26–31], little is still known about the actual dimensions of the anion-transporting pathway of the CFTR channel. There is not even a consensus about the number of CFTR molecules forming a single channel structure. Electron microscope studies of purified, antibody-decorated CFTR performed at 2-nm resolution revealed CFTR as a dimer of ellipsoidal form ($12 \times 10.6 \times 16.2$ nm) with orifices beneath the putative TMD [28]. Atomic force microscopy (AFM) of immunogold-labeled CFTR on isolated plasma membranes also revealed the CFTR channel as a tail-to-tail dimer with a central pore of unrealistically large ($\sim$10 nm) radius [32]. In contrast, single molecule fluorescence imaging in live cells [33] and electron microscopy of two-dimensional CFTR crystals [26] provided evidence for monomeric CFTR. The latter study visualized shafts (up to 1 nm in radius) across the CFTR protein [26]; however, their relationship to the actual path of anions traversing the CFTR protein remains unknown.

The poorly and non-hydrolyzable nucleotide analogs, including 5′-adenylylimidodiphosphate (AMP-PNP) and polyphosphate pyrophosphate (PPi), have been employed extensively for the investigation of the mechanisms underlying CFTR activation [1, 34]. The binding of AMP-PNP or PPi to NBDs causes the channels to become "locked" open [35–37] predominantly through effects at NBD2 preventing the channel closure [38]. This locked-open phenotype is also observed when the ATPase activity of NBD2 is abolished by the mutation of K1250A or E1371S [10, 23, 39]. However, there is little, if any, structural information of the CFTR pore as to the actual conformational change associated with transitions between the hydrolytic, open state and the non-hydrolytic, locked-open state.

Previous functional studies indicated that the CFTR pore in the open state exhibits an asymmetry in the permeability to large organic anions [19, 40–46] and that this unique functional asymmetry of the CFTR channel is disrupted in the locked-open state in the presence of a non-hydrolyzing ATP analog [21, 43, 47, 48]. Thus, there is a possibility that such functional properties of the CFTR channel are associated with changes in a structural asymmetry of the channel pore.

Here, we made systematical studies by using polymeric forms of ethylene glycol in the pore of a single CFTR $Cl^-$ channel to gauge the size of the pore entrance for the ionic transport pathway in the heterologously expressed channel protein for the following reasons. Polyethylene glycols (PEGs) in water solutions obey the viscosity law for random coils [49–51] and act as a "hard sphere" [52]. These organic nonelectrolytes should exhibit no coulombic interaction with the ion channel wall. Also, PEGs have been successfully used for single-channel pore sizing experiments both in lipid bilayer experiments [53, 54] and in patch-clamp studies [55, 56], yielding estimates consistent with X-ray crystallography and electron microscopy data [54]. The present study demonstrated that the CFTR channel has a highly asymmetric pore (with a larger cytoplasmic entrance) in the hydrolytic open state, and that this asymmetry is mostly lost by dilatation of the extracellular entrance in the non-hydrolytic, locked-open conformation induced by AMP-PNP.

Preliminary results have appeared in abstract form [57].

## Materials and methods

### Cells and transfection

Human embryonic kidney HEK293T cells were grown in DMEM supplemented with 10% fetal calf serum. The cells were plated on 35-mm dishes to obtain approximately

20–30% confluence on the day of transfection. For single-channel recordings, the cells cultured on glass coverslips were used.

The vector pBQ6.2 containing a full-length wild-type human CFTR cDNA insert was a kind gift from Dr. J.R. Riordan (University of North Carolina at Chapel Hill, NC, USA). The coding region of CFTR was subcloned into a bicistronic vector, pCINeo-IRES-GFP (a kind gift from Dr. J. Eggermont, KU Leuven, Belgium), to produce an expression vector [58]. Cells were transiently transfected with Effectene transfection reagent (Qiagen, Valencia, CA, USA) according to the manufacturer's instruction.

## Channel sizing

Studies on the permeability and open-channel blocking effects of negatively charged molecules may provide some information on the size of anion channel pore or vestibule. However, the interaction between these anionic molecules and charged sites within a channel pore should be affected by the applied transmembrane electric field. Moreover, there is more than one anion-binding site in the cytoplasmic vestibule [59] and some anion-interacting sites in the non-pore-lining amino acid side chains [60] of the CFTR channel. Therefore, in the present study, we gauged the size of the pore entrance of CFTR channel by studying partition of non-charged organic molecules, PEG 200–3,400, in the pore of a single CFTR channel.

In order to quantitatively analyze the differential polymer partitioning in the CFTR channel pore, we use the filling coefficient ($F$) defined according to our previous report [61]:

$$F = [(\gamma_O - \gamma)/\gamma]/[(\chi_O - \chi)/\chi] \quad (1)$$

where $\gamma$ and $\chi$ are the channel conductance and the bulk solution conductivity in the presence of nonelectrolytes, respectively, and $\gamma_O$ and $\chi_O$ are the same parameters in a control solution devoid of nonelectrolytes. This coefficient represents the fraction of the pore filled with the polymer and is based on the assumption that the pore electrical resistance can be considered as a sum of resistances of two parts in series: filled with polymer [with a resistance of $F/(A\chi)$) and non-filled (with a resistance of $F/(A\chi_O)$], where $A = \pi R_p^2/L$, $R_p$ is the pore radius and $L$ is the pore length.

## Solutions

The Ringer solution contained (in mM): 135 NaCl, 5 KCl, 2 $CaCl_2$, 1 $MgCl_2$, 5 Na-HEPES, 6 HEPES, and 5 glucose (pH 7.4, 290 mosmol/kg $H_2O$). The standard pipette solution contained (in mM): 146 NMDG, 2 $MgCl_2$, and 5 HEPES/HCl (pH 7.4, 280 ± 3 mosmol/kg $H_2O$). In the cell-attached mode, CFTR channels were activated by adding 1–5 μM forskolin to the bathing solution. In the inside-out configuration, the bathing solution was prepared by adding 2 mM ATP to the pipette solution, and the CFTR channels were activated by 5–25 U/ml PKA catalytic subunit (Promega, Madison, WI, USA) with 2 mM MgATP. In some inside-out experiments, the bath solution was supplemented with AMP-PNP (Li-salt: Sigma, St. Louis, MO, USA) at the concentration (5 mM) which was used in previous studies [26, 43]. For polymer partitioning experiments, the nonelectrolytes, PEG with a variety of molecular weights (PEG 3,400; ICN Biomedicals, Aurora, OH, USA; and all others from Wako Pure Chemical, Osaka, Japan), were added to pre-made solutions to a final concentration of 20% (wt/vol). The osmolality was measured using a freezing-point depression osmometer (OM802, Vogel, Germany). The bulk conductivity was measured using a B-173 conductivity meter (Horiba, Kyoto, Japan). The hydrodynamic radii ($R_h$) were taken from our previous report [55].

## Electrophysiology

Patch electrodes were fabricated from borosilicate glass capillaries using a laser micropipette puller (P-2000; Sutter Instruments, Novato, CA, USA). The tips of the electrodes were filled by immersing in the PEG-containing solution, and then the pipettes were back-filled with the same solution. Higher osmotic pressure generated by the nonelectrolytes added to the pipette solution greatly decreased the stability of patches formed using relatively wide 2- to 3-MΩ pipettes. However, when the pipette tip was smaller (4–7 MΩ) the patches survived long enough to perform accurate single-channel measurements in the presence of nonelectrolytes. Membrane currents were measured with an EPC-9 patch-clamp system (Heka-Electronics, Lambrecht/Pfalz, Germany). The membrane potential was controlled by shifting the pipette potential ($V_p$) and is reported as $-V_p$. Currents were filtered at 1 kHz and sampled at 5–10 kHz. The traces were further filtered off-line at 100–400 Hz for data analysis and presentation. Data acquisition and analysis were done using Pulse+PulseFit (Heka-Electronics). Liquid junction potentials were calculated according to Barry and Lynch [62] and were corrected either on- or off-line when appropriate. All experiments were performed at room temperature (23–25°C).

## Data analysis

Single-channel current amplitudes were measured either by manually placing a cursor at the open and closed channel levels or by constructing all-point histograms and fitting these with Gaussian functions. We only rarely observed

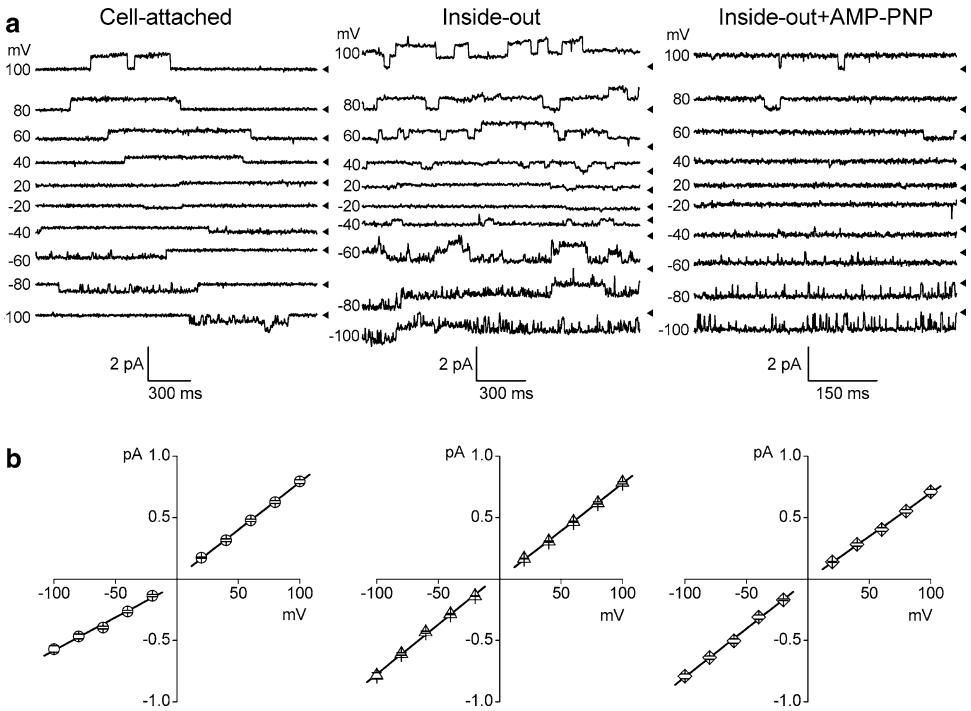


**Fig. 1** Single CFTR $Cl^-$ channel currents in the open and locked-open states recorded from HEK293T cells transiently transfected with CFTR gene. Representative current traces (**a**) and corresponding unitary current–voltage relationships (**b**) recorded from a cell-attached patch (*left traces*), inside-out patch (*center traces*) in the presence of 2 mM ATP and inside-out patch in the presence of 2 mM ATP + 5 mM AMP-PNP (*right traces*) in the bath (intracellular) solution with standard pipette solution at different membrane voltages as indicated on the *left of each trace*. *Arrowheads* on the *right of each trace* indicate zero current level. Each data point represents the mean ± SEM of 8–32 measurements from 5–7 different patches. *Solid lines* are linear fits with slopes corresponding to the unitary outward and inward conductances

such subconductance states of the channel as previously reported [63, 64]. In our experimental conditions using a HEPES buffer, however, current records through the above filter demonstrated the presence of two functionally different open states, named as O1 and O2 [23, 42], of the CFTR channel. These two states exhibited close single-channel conductances that were not easily distinguished. Moreover, one of the states (O2) is considerably shorter-lived than the other one [23]. With this in mind, the data of the present study are related to the longer-lived (O1) state. In the presence of AMP-PNP or PPi closing of the CFTR channel was rare and brief especially at negative potentials (see Fig. 1). This open state of the channel is known as non-hydrolytic, locked-open state which is referred to the O* state hereafter. For measurements of single-channel amplitude, the relatively long closing was used as a reference point. In the presence of several CFTR channels in the patch, all-point histograms were constructed, fitted with Gaussian functions, and the difference between positions of maximum values of the adjacent Gaussians was taken as the channel amplitude. The reversal potentials were calculated by fitting I–V curves to a second-order polynomial [55]. Data were analyzed using Origin, versions 5–7 (OriginLab, Northampton, MA, USA). Pooled data are given as mean ± SEM of $n$ observations. More than 5 measurements of the current amplitude of the events derived from at least 5 different patches were provided for calculation of the mean single-channel amplitude. Statistical differences in slopes of linear fits were evaluated by analysis of covariance using StatsDirect software (StatsDirect, Cheshire, UK) and considered significant at $P < 0.05$.

## Results

### Characteristics of single CFTR channels

Lack of endogenous expression of the CFTR protein in HEK293T cells has been confirmed previously by immunofluorescence microscopy using an anti-CFTR antibody raised against the intracellular R-domain [58]. Stimulation with an adenylyl cyclase activator, 1–5 μM forskolin, did not activate single-channel currents in non-transfected HEK293T cells ($n = 5$, data not shown). We introduced CFTR into HEK293T cells by transient transfection with a bicistronic expression vector containing GFP as a marker for positive selection of CFTR-expressing cells. We

previously showed that this results in expression of the CFTR protein, which can be detected by western blot analysis as a 180-kDa mature glycosylated band and recorded functionally as a large cAMP-activated whole-cell conductance with a linear current–voltage relationship and without exhibiting time-dependent activation or inactivation [58]. In the present experiments, we examined the single-channel activity in CFTR-transfected GFP-positive cells. The cell-attached patch recordings were mostly silent in non-stimulated conditions. Stimulation with forskolin after giga-ohm seal formation caused a high level of single-channel activity with relatively slow gating (Fig. 1a, left traces). The channel events had the mean unitary amplitudes of 0.79 ± 0.02 pA ($n = 14$) and −0.57 ± 0.03 pA ($n = 11$) at +100 and −100 mV, respectively. The unitary I–V relationship for these events exhibited slight outward rectification (Fig. 1b, left graph) due to not only an anion concentration gradient but also fast open-channel block by cytosolic organic anions [65] and had a reversal potential of −1.6 ± 1.3 mV. The mean slope conductances in the cell-attached mode were 7.76 ± 0.11 and 5.37 ± 0.32 pS at positive and negative potentials, respectively. The channel activity gradually disappeared after washing out forskolin or after patch excision unless the bath (intracellular) solution contained ATP. In the excised inside-out patches, the single-channel activity could be restored by bath-application of 5–25 U/ml PKA catalytic subunit and 2 mM MgATP (Fig. 1a, center traces). In the inside-out mode, the mean unitary amplitudes were 0.78 ± 0.01 pA ($n = 37$) and −0.79 ± 0.03 pA ($n = 11$) at +100 and −100 mV, respectively. The unitary I–V relationship for these events in the excised mode was linear and symmetrical (Fig. 1b, center graph) with reversal at 0 mV, and the mean slope conductances were 7.75 ± 0.12 and 8.10 ± 0.23 pS at positive and negative potentials, respectively. In the presence of 5 mM AMP-PNP together with 2 mM MgATP in the bath solution, we recorded more prolonged single-channel events (Fig. 1a, right traces), which reversed at 0 mV and had the mean slope conductances of 7.05 ± 0.17 and 7.88 ± 0.24 pS at positive and negative potentials, respectively, in the inside-out mode (Fig. 1b, right graph). Thus, these properties reproduce the phenotype of the CFTR $Cl^-$ channels observed earlier after heterologous expression in oocytes [25], mammalian cell lines [38, 66] and lipid bilayers [23, 67].

## Differential effects of polymers on the CFTR current amplitude

When the polymer-containing solutions were infused into the bath, they differentially affected the unitary currents of the pre-activated CFTR $Cl^-$ channels in inside-out patches depending on their molecular size, as illustrated in Fig. 2. Infusion of a small polymer, PEG 300 (hydrodynamic radius: $R_h = 0.53$ nm), reduced both the inward and outward currents from around 0.5 pA (Fig. 2a) to 0.2–0.3 pA (Fig. 2b) at ±60 mV. In contrast, a large polymeric molecule, PEG 2,000 ($R_h = 1.39$ nm), did not have such an effect on the unitary channel amplitude (Fig. 2c). Since the unitary current–voltage (I–V) relationship remained linear in both the negative and positive voltage ranges in the presence of PEGs, for further analysis of the polymer effects, we used slope conductances calculated separately for inward and outward unitary currents. The inward conductance was decreased significantly in the presence of PEG 300 to the value of 4.37 ± 0.18 pS (a 46% decrease from the control). The outward conductance was also decreased, albeit to a lesser extent of 32%. In contrast to PEG 300, the channel inward and outward conductances in the presence of PEG 2,000 (8.36 ± 0.26 and 7.93 ± 0.10 pS, respectively) were not significantly different from the control values (Fig. 2d). These results indicate that only a small molecule like PEG 300 was able to reach the channel interior to interfere with the movement of $Cl^-$ ions, whereas a larger molecule of PEG 2,000 was effectively excluded from the CFTR $Cl^-$ channel pore.

## Dimensions of the entrance of CFTR channel pore

In order to differentially assess the size of extracellular and intracellular entrances or vestibules of the CFTR $Cl^-$ channel pore, we systematically studied the effects of polymers of various molecular sizes ranging from 0.45 to 1.84 nm in the following five experimental configurations. Configuration 1: polymers applied from the extracellular side (pipette-application) in the cell-attached mode; configuration 2: polymers applied from the extracellular side (pipette-application) in the inside-out mode; configuration 3: polymers applied from the intracellular side (bath-application) in the inside-out mode; configuration 4: polymers applied from the extracellular side (pipette-application) in the inside-out mode in the presence of 5 mM AMP-PNP in the bath; and configuration 5: polymers applied from the intracellular side (bath-application) in the inside-out mode in the presence of 5 mM AMP-PNP in the bath.

All polymers tested efficiently decreased the bulk solution conductivity by about 50% (Fig. 3a, open squares). However, the larger molecules (PEG 1,540–3,400 of $R_h = 1.16$–$1.84$ nm) had no significant effect on the channel amplitude or the slope conductances in any of the experimental configurations (Fig. 3a). Thus, these molecules had no access to the channel interior and were completely excluded from the CFTR channel pore. The effects of smaller molecules depended on the sidedness of application. PEGs with $R_h \leq 0.95$ nm (PEG 300–1,000)

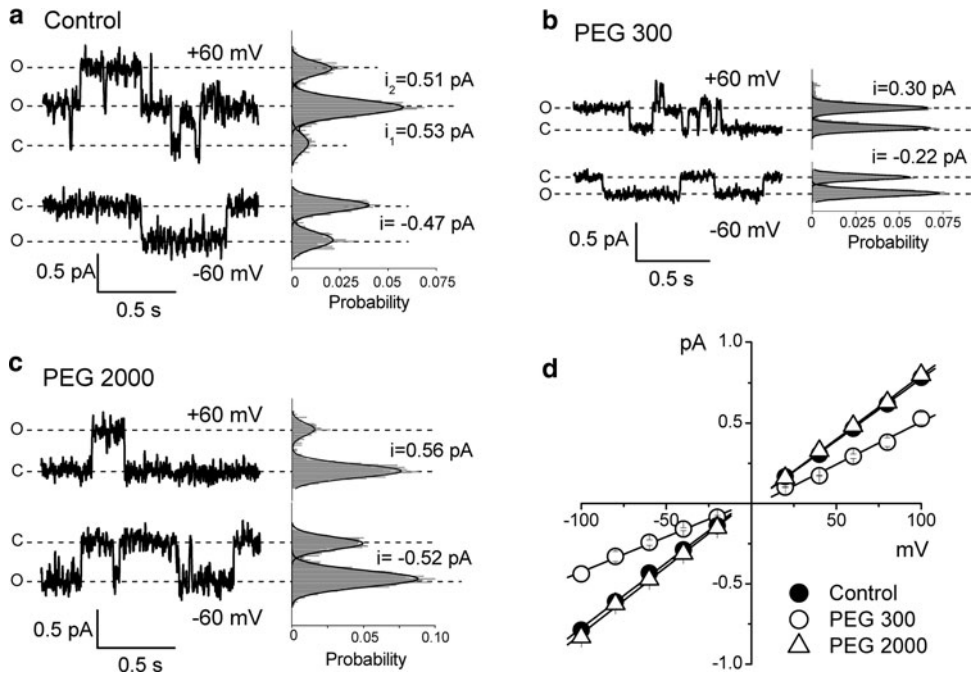


**Fig. 2** Effects of polyethylene glycols on the single CFTR $Cl^-$ channel currents. Representative current traces recorded from excised inside-out patches at +60 and at −60 mV in control conditions in the absence of nonelectrolytes (**a**) and in the presence of PEG 300 (**b**) and PEG 2,000 (**c**) in the bath solution. *C* denotes the closed state, *O* corresponds to the open channel level, respectively. The respective all-point histograms are shown at the right of each record; the histograms (*shadowed*) were fitted with Gaussians (*solid lines*) to give the peak-to-peak single-channel amplitudes (*i*) as indicated. Single-channel current–voltage relationships (**d**) were obtained in control conditions (*filled circles*) and in the presence of PEG 300 (*open circles*) and PEG 2,000 (*open triangles*) in the bath solution. Each data point represents the mean ± SEM of 5–29 measurements from 5–9 patches. *Solid lines* are linear fits with slopes corresponding to the unitary outward and inward conductances given in the text. The slope for PEG 300 is significantly different from the control slope at $P < 0.05$

significantly suppressed the inward conductance when applied from the intracellular side (filled circles), but only the molecules with $R_h \leq 0.62$ nm (PEG 200–400) were able to reduce the outward conductance when applied from the extracellular side (open circles and triangles). These data strongly suggest that the accessibility of the two vestibules of the CFTR channel pore to the polymeric probes is substantially different and that the effective size of the intracellular entrance is greater than that of the extracellular entrance. The radii of largest effective polymers, PEG 1,000 (0.95 nm) and PEG 400 (0.62 nm), give approximate estimates of the lowest limit of the size for intracellular and extracellular entrances of CFTR channel, respectively.

In the plot of filling coefficient (defined by Eq. 1) as a function of polymer hydrodynamic radius (Fig. 3b), the data points are separated into two distinct groups, the values of *F*(out) (open symbols) and *F*(in) (filled symbols), which correspond to extracellular and intracellular application of polymers, respectively. The two solid lines are linear fits to the data points of the descending part of the curve which represents a transition zone from partial filling ($0 < F < 1$) to complete exclusion ($F = 0$). The intersections of these two lines with the horizontal dashed line ($F = 0$, zero filling) give estimates of the cut-off size of the extracellular ($R1 = 0.70 \pm 0.16$ nm) and intracellular ($R2 = 1.19 \pm 0.02$ nm) entrances to the CFTR channel pore.

## Dilatation of the extracellular entrance to the CFTR channel pore induced by AMP-PNP

Linsdell and Hanrahan [43] described a unique property of CFTR channel to pass large organic anions when they were present on the intracellular, but not the extracellular, side. This asymmetry was not observed for small inorganic anions and was disrupted by inhibition of ATP hydrolysis in the presence of AMP-PNP or PPi [43]. In light of these reported observations, we hypothesized that the non-hydrolytic conformation of the CFTR channel is associated with dilatation of the extracellular entrance, thereby allowing passage of large organic anions from the extracellular side.

In the presence of AMP-PNP (5 mM) and ATP (2 mM) in the bath (intracellular) solution, the unitary I–V relationship showed a slight inward rectification with the mean slope conductances of 7.05 ± 0.17 and 7.88 ± 0.24 pS at positive and negative potentials, respectively, in the inside-out mode (Fig. 1b, right panels). Under these experimental conditions,

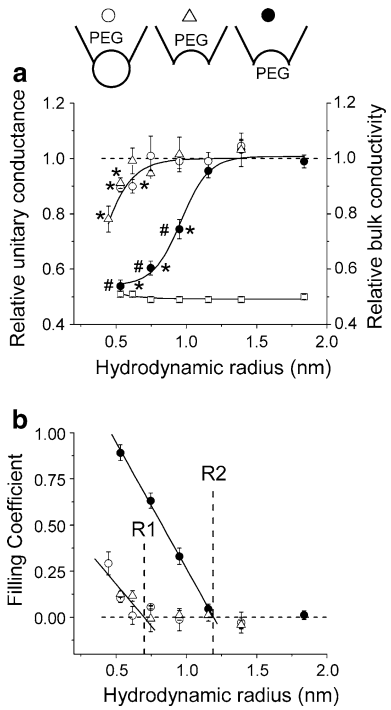


**Fig. 3** Effects of polymers on the single-channel conductance of the CFTR $Cl^-$ channel in the absence of AMP-PNP. **a** Relative changes in the unitary single-channel conductance (*left axis*) and bulk conductivity (*right axis*) as a function of the hydrodynamic radius ($R_h$) of PEG molecules ($R_h$ = 0.45, 0.53, 0.62, 0.75, 0.95, 1.16, 1.39 and 1.84 nm for PEG 200, 300, 400, 600, 1,000, 1,540, 2,000 and 3,400, respectively). *Filled circles* represent the inward slope conductance obtained in the inside-out mode with polymers added to the bath solution (configuration 3). *Open circles* and *open triangles* represent the outward slope conductance obtained with polymers added to the pipette solution in the inside-out mode (configuration 1) and the cell-attached mode (configuration 2), respectively. Data were collected from 5–9 different patches for each polymer. *Open squares* represent the relative decrease in the bulk conductivity of the solutions used in these experiments ($n = 5$). *Significantly different from the slope conductance obtained in control conditions without polymers at $P < 0.05$. #Significantly different from the respective slope conductance obtained with polymers added to the pipette solution in the inside-out mode at $P < 0.05$. *Inset* Schematic illustrations of configurations 1–3 used in these experiments. **b** Filling coefficients calculated according to Eq. 1 as a function of the hydrodynamic radius of PEG molecules. Symbols are the same as in (**a**). *Solid lines* are linear fits to the descending parts of the curves with correlation coefficient of −0.90 and −0.99 for extracellular and intracellular PEG application experiments, respectively. A *horizontal dashed line* corresponds to zero filling. *R*1 and *R*2 denote the radius of the extracellular and intracellular entrance of the CFTR $Cl^-$ channel pore, respectively

the polymers added from the extracellular side exhibited drastically different effects (Fig. 4a). Specifically, PEG 300–600 ($R_h$ = 0.53–0.75) caused significantly larger effects on the outward conductance (Fig. 4a, open diamonds) compared to its effects in the absence of AMP-PNP (Fig. 3a, open triangles). Examples of single-channel current recordings in the absence (upper trace) and presence (lower trace) of AMP-PNP in the bath (intracellular) solution for PEG 400 are shown in Fig. 4a (inset). These results suggest substantial widening of the extracellular entrance to the pore induced by AMP-PNP.

The plot of filling coefficient as a function of polymer hydrodynamic radius (Fig. 4b, open diamonds) yielded a radius $R3 = 0.93 \pm 0.23$ nm, indicating a pore size dilatation of about 25%. In contrast, the intracellular entrance was insensitive to the presence of AMP-PNP as evidenced by the similarity of the radius of $R4 = 1.15 \pm 0.08$ nm (Fig. 4b, filled diamonds) and $R2 = 1.19 \pm 0.02$ nm (Fig. 3b, filled circles), obtained when the polymers were added from the intracellular side of the CFTR channel in the presence and absence of AMP-PNP, respectively.

## Discussion

### Highly asymmetric structure of CFTR channel pore in the open state

The present work shows that the nonelectrolytes exclusion method (when used in the conditions where there is no interaction between nonelectrolyte and the channel) can be used successfully in single-channel patch-clamp experiments to study the geometry of ion channels with conductance as small as ~10 pS. In the case of CFTR, this method revealed that the channel has a highly asymmetric pore (with the cut-off radius of $1.19 \pm 0.02$ and $0.70 \pm 0.16$ nm for the cytoplasmic and the extracellular entrances, respectively) in the hydrolytic open state. The geometric asymmetry revealed in the present study by polymer partitioning is consistent with the functional asymmetry of CFTR $Cl^-$ channel suggested by blocking effects of large organic anions and osmolytes only from the intracellular but not the extracellular side of the pore [40, 41, 45, 65, 66, 68, 69], by asymmetric permeability to organic anions [43] and by intrinsic weak inward rectification [46]. The present results of an asymmetric ion transporting pathway with a wider intracellular entrance is also consistent with a teepee-like CFTR pore structure proposed by summarizing some of site-directed mutagenesis and ion permeation studies [21].

The predicted transmembrane topology for CFTR (where 79.5% of the whole CFTR molecule composes cytoplasmic domains [28–30]) might be related to its structural asymmetry. Such a highly asymmetric pore geometry of the CFTR channel with a narrower extracellular pore entrance is consistent with its close relationship to the ABC-exporters, which also have exceedingly asymmetric structures with a wide interior chamber to accommodate a variety of exporting substances [7]. In

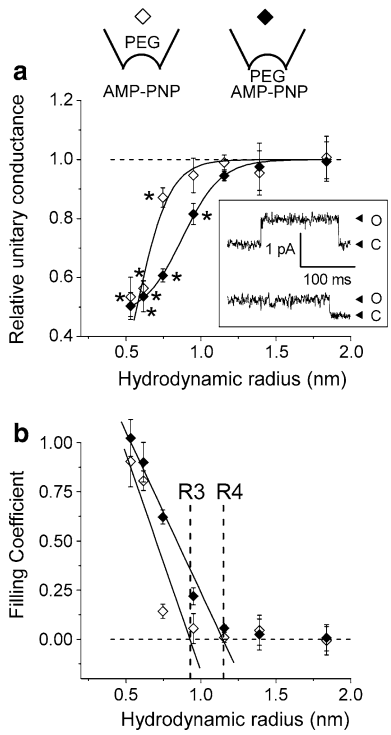


**Fig. 4** Effects of polymers on the single-channel conductance of the CFTR $Cl^-$ channel in the presence of AMP-PNP. **a** Relative changes in the unitary single-channel conductance as a function of the hydrodynamic radius of PEG molecules in the presence of AMP-PNP in the bath (intracellular) solution in the inside-out mode. *Open diamonds* represent the outward slope conductance obtained with polymers added to the pipette solution (configuration 4). *Filled diamonds* represent the inward slope conductance obtained with polymers added to the bath solution (configuration 5). Data were collected from 5–9 different patches for each polymer. *Significantly different from the slope conductance obtained in control conditions without polymers at $P < 0.05$. The slope conductances obtained in the presence of AMP-PNP for PEG 300, 400, 600 and 1,000 (*filled diamonds*) are significantly different from those in the absence of AMP-PNP (*open triangles* in Fig. 3a). *Upper inset* Schematic illustrations of configurations 4 and 5 used in this experiment. *Lower inset* Representative current traces recorded at +100 mV in the absence (*upper trace*) and presence (*lower trace*) of AMP-PNP in the bath (intracellular) solution. **b** Filling coefficients calculated according to Eq. 1 as a function of the hydrodynamic radius of PEG molecules. Symbols are the same as in (**a**). *Solid lines* are linear fits to the descending parts of the curves with correlation coefficient of −0.92 and −0.99 for extracellular and intracellular PEG application experiments, respectively. A *horizontal dashed line* corresponds to zero filling. *R*3 and *R*4 denote the radius of the extracellular and intracellular entrance, respectively, of the CFTR $Cl^-$ channel in the presence of AMP-PNP in the bath solution

addition, the cut-off sizes of the CFTR pore entrances estimated in the present study fit well with the dimensions of shafts visible in electron microscope images of crystals of purified CFTR protein [26, 27], suggesting that the shafts are closely associated with the anion-translocation pathway of CFTR $Cl^-$ channel.

The PEG-partition study allows us to estimate not only the cut-off size of the channel entrance from the hydrodynamic radii of accessible PEGs but also the channel pore geometry from the filling coefficients of the PEGs [52, 59, 68]. It is of importance that the small PEGs (e.g., PEG 300) filled the channel in a side-dependent manner. The $F$(out) and $F$(in) values were found to be equal to $0.11 \pm 0.02$ and $0.89 \pm 0.04$ for extracellular and intracellular PEG 300 applications, respectively (Fig. 3b). Such a difference would be caused, at least in part, by a higher access rate of PEG 300 from a wider intracellular side compared to a lower access rate from a narrow extracellular side. The simplest assumption would be that filling of the polymer was induced by simple diffusion and the $F$ value is proportional to the cross-sectional area of the channel entrance. This assumption yields $F$(in)/$F$(out) $\sim$ 1.8 for $R1 = 0.70$ and $R2 = 1.19$. However, the calculated ratio is considerably less than the actually measured ratio of about 8 for PEG 300.

A more prominent difference between $F$(in) and $F$(out) would be caused by an obstacle to polymer filling, if the obstacle exists far from the middle of the route of the channel pore. As PEG 300 ($R_h = 0.53$ nm) is not able to fill the CFTR pore completely, the obstacle squeezes the pore size down to ≤0.53 nm in radius. This is consistent with a fact that the apparent functional pore radius at the narrowest zone of CFTR channel was extrapolated down to 0.27 nm from anion permeability measurements [66]. Such an obstacle would restrict the access of PEG to the region behind the obstacle, thereby giving rise to physical separation of the higher-resistance pore region filled with this polymer from the lower-resistance region devoid of the polymer. Thus, the $F$(in)/$F$(out) value of around 8 for PEG 300 may suggest that the obstacle exists very much closer to the extracellular entrance. It seems feasible that a narrowest constriction within the pore serves as the obstacle for polymer nonelectrolytes. The definition of the filling coefficient is based on the assumption that the pore electrical resistance can be considered as a sum of resistances of two parts in series: filled with polymer and non-filled. Thus, it may be reasonable to imagine that the $F$ value electrophysiologically evaluated by Eq. 1, though not identical, can be related to the effective electrical distance for permeating $Cl^-$ ions. The linear I–V relationship of CFTR in the absence of PEG may imply that the applied voltage drops uniformly along the pore length. The value ($F = 0.11 \pm 0.02$) for the extracellular application would mean that only chloride ions moving 1/10 of the total voltage drop distance (the electrical distance) sense the presence of PEG added from the outside. Thus, the narrowest constriction as a barrier for PEG 300 is located not closer than 10% of the total electrical distance for chloride ions from the outside. Consistently, chloride ions moving up to approx. 90% from the intracellular mouth sense the presence of PEG 300 added from the intracellular side, as

evidenced by $F = 0.89 \pm 0.04$ for the case of intracellular application. Even if a difference in the polymer access rates at both entrances partially contributed to the difference between $F$(in) and $F$(out), it would be reasonable to conclude that the narrowest constriction of the CFTR channel pore exists closer to the extracellular entrance. Our results are consistent with previous reports suggesting that the binding sites for chloride and for negatively charged blockers exist near the extracellular side of CFTR $Cl^-$ channel pore [45, 66, 69].

On the basis of electron microscope images of two-dimensional crystals of purified CFTR protein [26, 27], it was considered that the CFTR pore has dual outer entrances. Although the dual-pore model explains well the existence of subconductance states of CFTR [23, 24, 42], we did not observe such distinct major levels of single-channel conductance frequently in the present study. In contrast, real time measurements of covalent modification of single R334C-CFTR channels by [2-(trimethylammonium)ethyl]methanethiosulfonate indicated that a single CFTR polypeptide forms a CFTR channel with a single pore [25]. Based on this single-pore hypothesis, the present results are summarized in Fig. 5 (left drawing) in a cartoon illustrating a possible CFTR conformation of the open state. In the absence of AMP-PNP, the open CFTR channel pore is highly asymmetric, exhibiting a narrower outer entrance with $R1 = 0.70$ nm and a wider inner entrance with $R2 = 1.19$ nm. The narrowest constriction, depicted in Fig. 5 (left drawing: smallest filled circle), may represent the selective filter and exhibit an apparent functional radius ($R5$) of 0.27 nm which was evaluated by studies of organic anion permeability by Linsdell et al. [66]. This state probably represents the O1 open state with a site in the pore to bind large cytoplasmic anions [41], which intermittently occlude $Cl^-$ flow resulting in bursts. Consistent with open-channel blocking studies [40, 41, 45, 65, 66, 68, 69], the CFTR pore geometry depicted in Fig. 5 allows access of bulky open-channel blockers, such as glibenclamide ($R_h \sim 0.63$ to 0.75 nm [45, 68]) and DIDS or DNDS ($R_h \sim 0.65$ nm [41]), to the pore only from the intracellular side.

## Dilating conformational change of CFTR channel pore in the locked-open state

It is well known that non-hydrolyzable nucleotide analogs considerably prolong the open channel bursts of CFTR in the presence of ATP [35, 36]. This state of the channel is called as non-hydrolytic, locked-open (O*) state. Using the PEG partitioning method, in the present study, we found that, in the presence of AMP-PNP, the geometry of the CFTR pore in the locked-open state is dramatically different from the O1 state. The cut-off radius of the outer

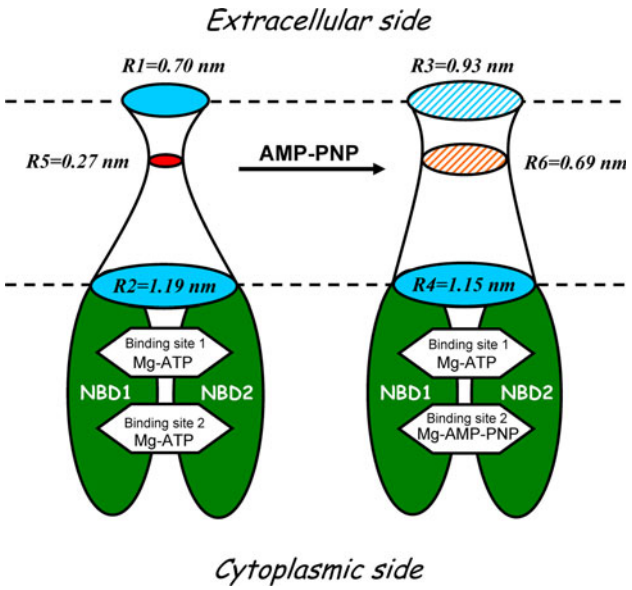


**Fig. 5** AMP-PMP-dependent structural transitions from the open state (O1) to the locked-open (O*) state of CFTR $Cl^-$ channel. *Left* A hypothetical drawing depicts the solute-accessible interior of a highly asymmetric pore with narrower extracellular (the radius of $R1 = 0.70$ nm) and wider intracellular ($R2 = 1.19$ nm) entrances in the presence of ATP and in the absence of AMP-PNP. The size of the narrowest constriction inside the pore (*smallest filled circle*, $R5 = 0.27$ nm) is based on the permeability data reported by Linsdell et al. [66]. *Right* A hypothetical drawing illustrates AMP-PNP-induced dilatation of the extracellular entrance ($R3 = 0.93$ nm) but not of the intracellular entrance ($R4 = 1.15$ nm) of the CFTR $Cl^-$ channel pore. *Smaller hatched circle* in the middle corresponds to an AMP-PNP-dependent widening of the narrowest constriction which may represent the selectivity filter. For the radius of the narrowest constriction in the presence of AMP-PNP, the value of $R6 = 0.69$ nm reported by Linsdell and Hanrahan [43] is adopted, and its localization in the proximity to the extracellular entrance of the channel is based on the present PEG partition study. *NBD1* and *NBD2* denote two nucleotide-binding domains of CFTR channel protein. The transmembrane and regulatory domains are not depicted for the simplicity

entrance ($R3$) became considerably larger (from 0.70 to 0.93 nm in radius). Moreover, PEG 300 was able to fill the channel in the presence of AMP-PNP in a manner nearly independent of the sidedness of the PEG application [$F$(out) $= 0.90 \pm 0.13$ and $F$(in) $= 1.02 \pm 0.09$] (Fig. 4b). As schematically depicted in Fig. 5 (right drawing), it thus appears that the structural asymmetry of CFTR channel pore became smoothed out by dilatation of the extracellular entrance of CFTR channel in the presence of AMP-PNP or PPi. The present finding is consistent with electron microscope studies of two-dimensional crystals of purified CFTR [26, 27] where the size of the supposed extracellular pore entrance at the channel structure obtained in the presence of AMP-PNP appears larger than that in the presence of Mg-ATP. Anion permeability experiments [43] also showed that ATPase inhibitors that lock CFTR channels in the open state (PPi, AMP-PNP), but not those that reduce channel open

probability ($NaN_3$, ADP), can considerably decrease the asymmetry in CFTR channel permeability to large anions: the radius of its narrowest constriction site (*R6*) was found to widen to 0.69 nm (this value is incorporated into Fig. 5, right drawing: smaller hatched circle). Thus, the cumulative data indicate that CFTR, which has not only a functionally but also a structurally asymmetric pore in the O1 state (Fig. 5, left drawing), exhibits a conformational change manifested by not only relaxation of the narrowest constriction but also dilatation of the extracellular entrance in association with the O* state in the presence of a non-hydrolyzable ATP analog (Fig. 5, right drawing). An intriguing question as to whether the mutation at the site essential for ATP hydrolysis in NBD2 (such as K1250A and E1371S) causes a similar conformational change remains for future studies. However, it must be noted that mutations (even in the non-pore region) themselves could alter the pore architecture of CFTR [70–72].

The asymmetry of $F$(out) and $F$(in) almost disappears for small PEG 300 and PEG 400 in the presence of AMP-PNP. However, the filling coefficient for PEG 600 was asymmetric for the two vestibules in the locked-open state [$F(\text{out}) = 0.14 \pm 0.04$, $F(\text{in}) = 0.62 \pm 0.04$], suggesting that the narrowest constriction site still exists near the extracellular side. Since a linear fitting of the open symbols (especially, the data point for PEG 600) in Fig. 4b looks poor, in Fig. 5 (right drawing), we tentatively depict the selectivity filter at the same location as for the conformation in the absence of AMP-PNP (left drawing).

The dilatation of the extracellular entrance and relaxation of the narrowest constriction may favor the increase in the single-channel conductance. However, it is well known that the single-channel conductance at the open and locked-open states are practically the same (e.g., [22, 36]) and not largely different in the present study (see Fig. 1b). The increase in cut-off radius of the extracellular entrance (without decreasing the size of intracellular entrance) and relaxation of the narrowest constriction of the CFTR pore may not necessarily be accompanied by an increase in the single-channel conductance, if the rate of ion permeation through the O1 state open CFTR channel is essentially identical to that through the O* state locked-open channel due to a conformational change resulting in a change in the profile of energy barriers within the pore.

There are, at least, two models of CFTR channel which are currently discussed by the scientific community (see, e.g., [24]): single-pore and dual-pore models. Several previous studies demonstrated that the CFTR pore exhibits more than two conformations displaying a number of subconductance levels [23, 24, 42]. Thus, it is likely that there are conformations other than closed, open and locked-open states in association with different subconductance levels of the CFTR channel regardless of a single-pore or dual-pore hypothesis. The structural basis for these subconductance states remains for future studies. The data obtained in the present study demonstrated a prominent difference in structure between open (O1) and locked-open (O*) states. Thus, an important implication of the present study is that there may be significant structural diversity even among different "open states".

**Acknowledgments** The authors would like to thank A.F. James (University of Bristol, UK) and Y. Sohma (Keio University, Tokyo) for helpful suggestions, E.L. Lee for reviewing the manuscript, T. Okayasu for secretarial help as well as M. Ohara and K. Shigemoto for technical support. This work was supported by Grants-in-Aid for Scientific Research (A) and (C) to Y.O. and R.Z.S. from the MEXT of Japan. We acknowledge a visiting Professorship from the Japanese Government and a support from CNPq (Brazil) to O.V.K.

## References

1. Vergani P, Nairn AC, Gadsby DC (2003) On the mechanism of MgATP-dependent gating of CFTR $Cl^-$ channels. J Gen Physiol 121:17–36
2. Kidd JF, Kogan I, Bear CE (2004) Molecular basis for the chloride channel activity of cystic fibrosis transmembrane conductance regulator and the consequences of disease-causing mutations. Curr Top Dev Biol 60:215–246
3. Riordan JR (2005) Assembly of functional CFTR chloride channels. Annu Rev Physiol 67:701–718
4. Gadsby DC, Vergani P, Csanady L (2006) The ABC protein turned chloride channel whose failure causes cystic fibrosis. Nature 440:477–483
5. Guggino WB, Stanton BA (2006) New insights into cystic fibrosis: molecular switches that regulate CFTR. Nat Rev Mol Cell Biol 7:426–436
6. Mense M, Vergani P, White DM, Altberg G, Nairn AC, Gadsby DC (2006) In vivo phosphorylation of CFTR promotes formation of a nucleotide-binding domain heterodimer. EMBO J 25:4728–4739
7. Higgins CF (2007) Multiple molecular mechanisms for multidrug resistance transporters. Nature 446:749–757
8. Aleksandrov AA, Aleksandrov LA, Riordan JR (2007) CFTR (ABCC7) is a hydrolyzable-ligand-gated channel. Pflugers Arch 453:693–702
9. Hanrahan JW, Wioland MA (2004) Revisiting cystic fibrosis transmembrane conductance regulator structure and function. Proc Am Thorac Soc 1:17–21
10. Vergani P, Lockless SW, Nairn AC, Gadsby DC (2005) CFTR channel opening by ATP-driven tight dimerization of its nucleotide-binding domains. Nature 433:876–880
11. Aleksandrov AA, Cui L, Riordan JR (2009) Relationship between nucleotide binding and ion channel gating in cystic fibrosis transmembrane conductance regulator. J Physiol 587:2875–2886
12. Muallem D, Vergani P (2009) ATP hydrolysis-driven gating in cystic fibrosis transmembrane conductance regulator. Philos Trans R Soc Lond B 364:247–255
13. Aleksandrov AA, Riordan JR (2001) CFTR as a ligand gated channel. Biophys J 80:470A
14. Shimizu H, Yu YC, Kono K, Kubota T, Yasui M, Li M, Hwang TC, Sohma Y (2010) A stable ATP binding to the nucleotide binding domain is important for reliable gating cycle in an ABC transporter CFTR. J Physiol Sci 60:353–362
15. Quinton PM (1999) Physiological basis of cystic fibrosis: a historical perspective. Physiol Rev 79:S3–S22

16. Sheppard DN, Welsh MJ (1999) Structure and function of the CFTR chloride channel. Physiol Rev 79:S23–S45
17. Ishiguro H, Steward MC, Naruse S, Ko SB, Goto H, Case RM et al (2009) CFTR functions as a bicarbonate channel in pancreatic duct cells. J Gen Physiol 133:315–326
18. Tang L, Fatehi M, Linsdell P (2009) Mechanism of direct bicarbonate transport by the CFTR anion channel. J Cyst Fibros 8:115–121
19. Liu X, Smith SS, Dawson DC (2003) CFTR: what's it like inside the pore? J Exp Zool A Comp Exp Biol 300:69–75
20. Linsdell P (2006) Mechanism of chloride permeation in the cystic fibrosis transmembrane conductance regulator chloride channel. Exp Physiol 91:123–129
21. McCarty NA (2000) Permeation through the CFTR chloride channel. J Exp Biol 203:1947–1962
22. Jordan IK, Kota KC, Cui GY, Thompson CH, McCarty NA (2008) Evolutionary and functional divergence between the cystic fibrosis transmembrane conductance regulator and related ATP-binding cassette transporters. Proc Natl Acad Sci USA 105:18865–18870
23. Gunderson KL, Kopito RR (1995) Conformational states of CFTR associated with channel gating: the role ATP binding and hydrolysis. Cell 82:231–239
24. Yue HW, Devidas S, Guggino WB (2000) The two halves of CFTR form a dual-pore ion channel. J Biol Chem 275:10030–10034
25. Zhang ZR, Cui G, Liu X, Song B, Dawson DC, McCarty NA (2005) Determination of the functional unit of the cystic fibrosis transmembrane conductance regulator chloride channel. One polypeptide forms one pore. J Biol Chem 280:458–468
26. Rosenberg MF, Kamis AB, Aleksandrov LA, Ford RC, Riordan JR (2004) Purification and crystallization of the cystic fibrosis transmembrane conductance regulator (CFTR). J Biol Chem 279:39051–39057
27. Awayn NH, Rosenberg MF, Kamis AB, Aleksandrov LA, Riordan JR, Ford RC (2005) Crystallographic and single-particle analyses of native- and nucleotide-bound forms of the cystic fibrosis transmembrane conductance regulator (CFTR) protein. Biochem Soc Trans 33:996–999
28. Mio K, Ogura T, Mio M, Shimizu H, Hwang TC, Sato C et al (2008) Three-dimensional reconstruction of human cystic fibrosis transmembrane conductance regulator chloride channel revealed an ellipsoidal structure with orifices beneath the putative transmembrane domain. J Biol Chem 283:30300–30310
29. Mornon JP, Lehn P, Callebaut I (2008) Atomic model of human cystic fibrosis transmembrane conductance regulator: membrane-spanning domains and coupling interfaces. Cell Mol Life Sci 65:2594–2612
30. Serohijos AWR, Hegedus T, Aleksandrov AA, He L, Cui L, Dokholyan NV et al (2008) Phenylalanine-508 mediates a cytoplasmic-membrane domain contact in the CFTR 3D structure crucial to assembly and channel function. Proc Natl Acad Sci USA 105:3256–3261
31. Zhang L, Aleksandrov LA, Zhao Z, Birtley JR, Riordan JR, Ford RC (2009) Architecture of the cystic fibrosis transmembrane conductance regulator protein and structural changes associated with phosphorylation and nucleotide binding. J Struct Biol 167:242–251
32. Schillers H (2008) Imaging CFTR in its native environment. Pflugers Arch 456:163–177
33. Haggie PM, Verkman AS (2008) Monomeric CFTR in plasma membranes in live cells revealed by single molecule fluorescence imaging. J Biol Chem 283:23510–23513
34. Aleksandrov AA, Chang X, Aleksandrov L, Riordan JR (2000) The non-hydrolytic pathway of cystic fibrosis transmembrane conductance regulator ion channel gating. J Physiol 528:259–265
35. Gunderson KL, Kopito RR (1994) Effects of pyrophosphate and nucleotide analogs suggest a role for ATP hydrolysis in cystic fibrosis transmembrane regulator channel gating. J Biol Chem 269:19349–19353
36. Hwang TC, Nagel G, Nairn AC, Gadsby DC (1994) Regulation of the gating of cystic fibrosis transmembrane conductance regulator C1 channels by phosphorylation and ATP hydrolysis. Proc Natl Acad Sci USA 91:4698–4702
37. Carson MR, Winter MC, Travis SM, Welsh MJ (1995) Pyrophosphate stimulates wild-type and mutant cystic fibrosis transmembrane conductance regulator $Cl^-$ channels. J Biol Chem 270:20466–20472
38. Carson MR, Travis SM, Welsh MJ (1995) The two nucleotide-binding domains of cystic fibrosis transmembrane conductance regulator (CFTR) have distinct functions in controlling channel activity. J Biol Chem 270:1711–1717
39. Ramjeesingh M, Li C, Garami E, Huan LJ, Galley K, Wang Y et al (1999) Walker mutations reveal loose relationship between catalytic and channel-gating activities of purified CFTR (cystic fibrosis transmembrane conductance regulator). Biochemistry 38:1463–1468
40. Linsdell P, Hanrahan JW (1996) Flickery block of single CFTR chloride channels by intracellular anions and osmolytes. Am J Physiol Cell Physiol 40:C628–C634
41. Linsdell P, Hanrahan JW (1996) Disulphonic stilbene block of cystic fibrosis transmembrane conductance regulator $Cl^-$ channels expressed in a mammalian cell line and its regulation by a critical pore residue. J Physiol 496:687–693
42. Ishihara H, Welsh MJ (1997) Block by MOPS reveals a conformation change in the CFTR pore produced by ATP hydrolysis. Am J Physiol Cell Physiol 273:C1278–C1289
43. Linsdell P, Hanrahan JW (1998) Adenosine triphosphate-dependent asymmetry of anion permeation in the cystic fibrosis transmembrane conductance regulator chloride channel. J Gen Physiol 111:601–614
44. Gupta J, Evagelidis A, Hanrahan JW, Linsdell P (2001) Asymmetric structure of the cystic fibrosis transmembrane conductance regulator chloride channel pore suggested by mutagenesis of the twelfth transmembrane region. Biochemistry 40:6620–6627
45. Zhou Z, Hu S, Hwang TC (2002) Probing an open CFTR pore with organic anion blockers. J Gen Physiol 120:647–662
46. Cai ZW, Scott-Ward TS, Sheppard DN (2003) Voltage-dependent gating of the cystic fibrosis transmembrane conductance regulator $Cl^-$ channel. J Gen Physiol 122:605–620
47. Zhang ZR, McDonough SI, McCarty NA (2000) Interaction between permeation and gating in a putative pore domain mutant in the cystic fibrosis transmembrane conductance regulator. Biophys J 79:298–313
48. Kogan I, Ramjeesingh M, Li C, Kidd JF, Wang YC, Leslie EM et al (2003) CFTR directly mediates nucleotide-regulated glutathione flux. EMBO J 22:1981–1989
49. Sabirov RZ, Krasilnikov OV, Ternovsky VI, Merzliak PG (1991) Influence of some nonelectrolytes on conductance of bulk solution and conductivity of ion channel—determination of pore radius from electric measurements. Biol Membr 8:280–291
50. Krasilnikov OV, Sabirov RZ, Ternovsky VI, Merzliak PG, Muratkhodjaev JN (1992) A simple method for the determination of the pore radius of ion channels in planar lipid bilayer membranes. FEMS Microbiol Immunol 5:93–100
51. Sabirov RZ, Krasilnikov OV, Ternovsky VI, Merzliak PG (1993) Relation between ionic channel conductance and conductivity of media containing different nonelectrolytes. A novel method of pore size determination. Gen Physiol Biophys 12:95–111
52. Merzlyak PG, Yuldasheva LN, Rodrigues CG, Carneiro CMM, Krasilnikov OV, Bezrukov SM (1999) Polymeric nonelectrolytes

to probe pore geometry: application to the α-toxin transmembrane channel. Biophys J 77:3023–3033
53. Bezrukov SM, Kasianowicz JJ (2002) Dynamic partitioning of neutral polymers into a single ion channel. In: Kasianowicz JJ, Kellermayer MSZ, Deamer DW (eds) Structure and dynamics of confined polymers. Kluwer, Dordrecht
54. Krasilnikov OV (2002) Sizing channels with neutral polymers. In: Kasianowicz JJ, Kellermayer MSZ, Deamer DW (eds) Structure and dynamics of confined polymers. Kluwer, Dordrecht
55. Sabirov RZ, Okada Y (2004) Wide nanoscopic pore of maxi-anion channel suits its function as an ATP-conductive pathway. Biophys J 87:1672–1685
56. Ternovsky VI, Okada Y, Sabirov RZ (2004) Sizing the pore of the volume-sensitive anion channel by differential polymer partitioning. FEBS Lett 576:433–436
57. Sabirov RZ, Ternovsky VI, Krasilnikov OV, Okada Y (2009) Gauging the pore size of three putative ATP releasing pathways by polymer partitioning. J Physiol Sci 59:S392
58. Ando-Akatsuka Y, Abdullaev IF, Lee EL, Okada Y, Sabirov RZ (2002) Down-regulation of volume-sensitive $Cl^-$ channels by CFTR is mediated by the second nucleotide-binding domain. Pflugers Arch 445:177–186
59. St Aubin CN, Zhou JJ, Linsdell P (2007) Identification of a second blocker binding site at the cytoplasmic mouth of the cystic fibrosis transmembrane conductance regulator chloride channel pore. Mol Pharmacol 71:1360–1368
60. Linsdell P, Zheng SX, Hanrahan JW (1998) Non-pore lining amino acid side chains influence anion selectivity of the human CFTR $Cl^-$ channel expressed in mammalian cell lines. J Physiol 512:1–16
61. Krasilnikov OV, Da Cruz JB, Yuldasheva LN, Varanda WA, Nogueira RA (1998) A novel approach to study the geometry of the water lumen of ion channels: colicin Ia channels in planar lipid bilayers. J Membr Biol 161:83–92
62. Barry PH, Lynch JW (1991) Liquid junction potentials and small-cell effects in patch-clamp analysis. J Membr Biol 121:101–117
63. Tao T, Xie JX, Drumm ML, Zhao JY, Davis PB, Ma JJ (1996) Slow conversions among subconductance states of cystic fibrosis transmembrane conductance regulator chloride channel. Biophys J 70:743–753
64. Bompadre SG, Cho JH, Wang X, Zou X, Sohma Y, Li M et al (2005) CFTR gating II: effects of nucleotide binding on the stability of open states. J Gen Physiol 125:377–394
65. Linsdell P, Hanrahan JW (1999) Substrates of multidrug resistance-associated proteins block the cystic fibrosis transmembrane conductance regulator chloride channel. Br J Pharmacol 126:1471–1477
66. Linsdell P, Tabcharani JA, Rommens JM, Hou YX, Chang XB, Tsui LC et al (1997) Permeability of wild-type and mutant cystic fibrosis transmembrane conductance regulator chloride channels to polyatomic anions. J Gen Physiol 110:355–364
67. Aleksandrov AA, Aleksandrov L, Riordan JR (2002) Nucleoside triphosphate pentose ring impact on CFTR gating and hydrolysis. FEBS Lett 518:183–188
68. Sheppard DN, Robinson KA (1997) Mechanism of glibenclamide inhibition of cystic fibrosis transmembrane conductance regulator $Cl^-$ channels expressed in a murine cell line. J Physiol 503:333–346
69. Linsdell P (2005) Location of a common inhibitor binding site in the cytoplasmic vestibule of the cystic fibrosis transmembrane conductance regulator chloride channel pore. J Biol Chem 280:8945–8950
70. Cotten JF, Welsh MJ (1999) Cystic fibrosis-associated mutations at arginine 347 alter the pore architecture of CFTR—evidence for disruption of a salt bridge. J Biol Chem 274:5429–5435
71. Cui G, Zhang ZR, O'Brien ARW, Song B, McCarty NA (2008) Mutations at arginine 352 alter the pore architecture of CFTR. J Membr Biol 222:91–106
72. Zhou JJ, Fatehi M, Linsdell P (2007) Direct and indirect effects of mutations at the outer mouth of the cystic fibrosis transmembrane conductance regulator chloride channel pore. J Membr Biol 216:129–142